

RESEARCH ARTICLE SUMMARY

BIOPHYSICS

Single-molecule dissection of stacking forces in DNA

Fabian Kilchherr, Christian Wachauf, Benjamin Pelz, Matthias Rief,
Martin Zacharias, Hendrik Dietz*

INTRODUCTION: In DNA double helices, hydrogen bonds connect the base pairs across the two strands, and stacking bonds act along the helical axis between neighboring base pairs. Our understanding of DNA and the way it is processed in biology would profit from improved knowledge about the elementary bonds in DNA. Detailed knowledge of the time scales for breaking and forming individual base pairs and base-pair stacks would also help to make more informed decisions in the design of dynamic DNA-based nanoscale devices.

RATIONALE: The goal of this work is to measure the dynamics of DNA base-pair stacking at the level of individual base-pair steps. Because stacking interactions act perpendicularly to the hydrogen bonds, it should be possible to use mechanical forces to break stacking while leaving hydrogen bonds intact. To realize such measurements, we combine the positioning capabilities of DNA origami with single-molecule manipulation, as enabled by dual-beam optical traps. To make the weak single-base-pair stacking interactions experimentally accessible, we prepared parallel arrays of blunt-end DNA dou-

ble helices to take advantage of avidity effects when these arrays form stacking interactions (see the figure). Our design allowed controlling the number and the sequences of the base-pair stacks. Noise-suppressing by stiff DNA origami beams connected by a flexible polymer tether enabled the repeated detection of unbinding and rebinding of stacking contacts at low forces (down to 2 piconewtons) with high time resolution (up to 1 kHz).

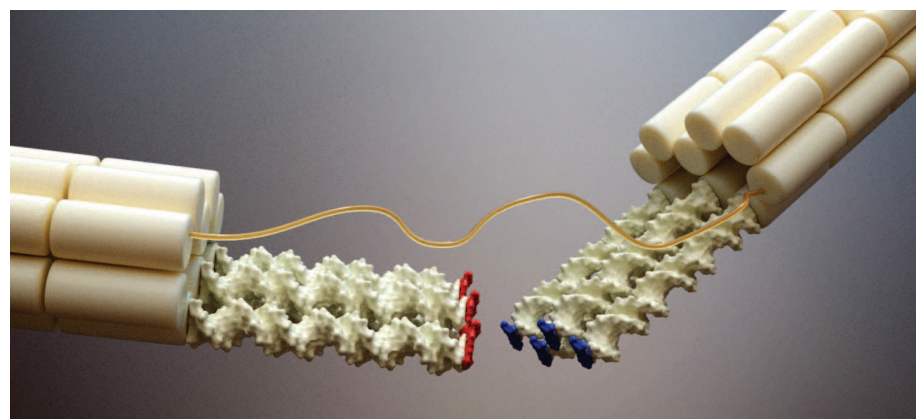
RESULTS: We sampled all 16 sequence combinations of installing a particular interfacial base pair on the array on the left beam and another base pair in the array on the right beam, and we created arrays with two, four, and six blunt ends. We could measure the force-dependent lifetimes for all base-pair step sequence combinations in the presence of 20 mM MgCl₂, which is a condition typically used in DNA nanotechnology. For a subset of base-pair step combinations, we also obtained data in the presence of 500 mM NaCl, which mimics the conditions in the cell nucleus. The base-pair stack arrays spontaneously dissociated at average rates ranging from 0.02 to 500 per second, where the dissociation time

scale strongly depended on the sequence combination and the stack array size. For a given sequence combination, larger array sizes always had larger lifetimes, as expected from avidity. Another key feature revealed in the lifetime data was the low sensitivity of the stacking interactions on the extent of pulling force. This phenomenon reflects short-ranged interaction potentials. Concerning rebinding of the stack arrays, we found that the rebinding kinetics depended much more strongly on the applied force, which may be understood by considering that rebinding of the stacks requires a thermally activated contraction of the

flexible tether—which was the same for all variants—against an opposing force tether contraction. However, the rebinding kinetics was independent, within

experimental error, of the base-pair step sequence combination and the size of the array under study. We used a model to estimate the free-energy increments per single base-pair stack from the kinetic rates that we measured with stack arrays. The free-energy increments per stack ranged from -0.8 to -3.4 kilocalories per mole. Our data reveals a trend in the stacking-strength hierarchy that may be associated with the extent of geometrical atomic overlap between the bases within a base-pair step.

CONCLUSION: Our data provides a quantitative basis for the rational design of dynamic DNA-based nanoscale machines and assemblies. Nanoengineers can directly read off the expected lifetimes of stack arrays for all sequence combinations and for various array sizes and at salt conditions that are commonly used in the field. With this data, design solutions for transition kinetics may be generated that cover several orders of magnitudes in lifetime, from milliseconds to several seconds. The sequence-resolved information obtained in our experiments may inform kinetic models of DNA hybridization and may help in adjusting force fields to perform more realistic molecular dynamics simulations. More generally, our experimental methods advance the capabilities of single-molecule mechanical experiments. Using the tethered-beam system, target molecules may be placed and exposed in controlled orientations and stoichiometry so as to study the weak forces occurring between them in solution. A variety of interactions between various kinds of molecules may be studied in the future due to the modularity and the addressability of the DNA origami-based tethered-beam system. ■



How strong is DNA base-pair stacking? Schematic illustration of the experimental system to measure the strength of base-pair stacking on the level of single particles. The system consists of two tethered DNA origami beams that feature parallel arrays of blunt-end DNA double helices. The beams may be attached to two micrometer-sized beads for manipulation in a dual-beam optical trap. With this system, we could measure lifetimes at which DNA base-pair stacks spontaneously dissociate as a function of force applied in the helical direction.

The list of author affiliations is available in the full article online.

*Corresponding author. Email: dietz@tum.de

Cite this article as F. Kilchherr et al., *Science* **353**, aaf5508 (2016). DOI: 10.1126/science.aaf5508

RESEARCH ARTICLE

BIOPHYSICS

Single-molecule dissection of stacking forces in DNA

Fabian Kilchherr,¹ Christian Wachauf,¹ Benjamin Pelz,² Matthias Rief,^{2,4}
Martin Zacharias,^{3,4} Hendrik Dietz^{1,4,5*}

We directly measured at the single-molecule level the forces and lifetimes of DNA base-pair stacking interactions for all stack sequence combinations. Our experimental approach combined dual-beam optical tweezers with DNA origami components to allow positioning of blunt-end DNA helices so that the weak stacking force could be isolated. Base-pair stack arrays that lacked a covalent backbone connection spontaneously dissociated at average rates ranging from 0.02 to 500 per second, depending on the sequence combination and stack array size. Forces in the range from 2 to 8 piconewtons that act along the helical direction only mildly accelerated the stochastic unstacking process. The free-energy increments per stack that we estimate from the measured forward and backward kinetic rates ranged from -0.8 to -3.4 kilocalories per mole, depending on the sequence combination. Our data contributes to understanding the mechanics of DNA processing in biology, and it is helpful for designing the kinetics of DNA-based nanoscale devices according to user specifications.

The processing of genetic information relies on the forces and energies underlying base-pair interactions in DNA. Hydrogen bonds connect the two Watson-Crick base pairs AT and GC across the two strands (1), and stacking forces act along the helical axis between neighboring base pairs (2) (Fig. 1A). Various spectroscopic techniques have been used to study the dynamics of DNA molecules, including the opening and flipping of mismatched bases (3, 4). The local and global dynamics of DNA is, however, determined by many contributions of base-pairing, stacking, and backbone interactions. In particular, the force-dependent time scales of breaking and reforming single base pairs and single base-pair stacks remain experimentally unexplored. At present, we do not know to which extent enzymes such as polymerases have to use actual force to break base pairs and base-pair stacks to process DNA. Furthermore, the time scales of these elementary bond-breaking and bond-forming steps ultimately determine the kinetics of nanotechnological devices and machines currently being developed from DNA (5–7). The goal of this work is to measure the dynamics of DNA base-pair stacking at the level of individual base-pair steps.

Because stacking interactions act perpendicularly to the hydrogen bonds, it should be possible to use mechanical forces to break stacking while leaving hydrogen bonds intact. We thus combine the capabilities of DNA nanotechnology, which allow positioning of molecules with atomic precision (8), with single-molecule force spectroscopy to manipulate molecular interactions in controlled spatial directions. Previous single-molecule mechanical assays based on atomic force microscopy (9, 10), optical traps (11–14), and magnetic tweezers (15–17) have provided important insight into the mechanics of DNA and into the folding energy landscapes of DNA secondary structures (18–20). However, the previous experiments measured the total contribution of all interactions stabilizing long DNA duplexes and lacked the control to break or form individual DNA base-pair steps.

Results

Experimental design

To enable a direct mechanical investigation of base-pair stacking forces on the level of individual DNA base pairs (Fig. 1A), without breaking hydrogen bonds, we have combined the molecular-level positioning capabilities of DNA origami-based nanotechnology (21–23) with the single-molecule manipulation capabilities of a dual-beam optical trap (24) (Fig. 1). Our experimental design integrates three components: (i) parallel arrays of base-pair stacks to rationally exploit avidity effects (Fig. 1B) for moving the weak individual stacking interactions into the force regimes and time scales that are experimentally accessible for the optical trap; (ii) stiff DNA beams to link the stack arrays to the optically trapped beads (Fig. 1C), where the beams have noise-suppressing

capabilities (20) to support the detection of unbinding and rebinding events occurring at extremely low forces (down to 2 pN) with fast kinetics (up to 1 kHz); (iii) a user-defined flexible tether linking the two beams (Fig. 1C), which enables the repeated observation and classification of unbinding and rebinding events, as seen previously with peptide linkers (25, 26) and long duplex DNA loops (27).

Design details of blunt-end arrays

The 10-helix DNA origami beams that we used in our experiments had persistence lengths p well above 3.5 μm (20) at a total length L of 250 nm per beam. Based on the high tangent angle correlation according to $\exp(-L/p)$, the beams were thus firmly in the rigid rod regime. The cantilevered blunt-end duplex DNA segments typically had a length of around three to four helical turns. Within the arrays of cantilevered, blunt-end DNA double helices (Fig. 1C, insets), the protruding helices were also coupled via lateral strand linkages to minimize translations and rotations of the interfacial blunt ends (fig. S1) (28). Given the persistence length of single-duplex DNA, which is on the order of 15 helical turns, and ignoring the fact that the cantilevered segments were further stabilized by lateral coupling, the protruding blunt-end arrays were also in the rigid rod regime. The cantilevered helices on the two opposing beam interfaces were also designed to be in helical register. Our design thus templates the formation of backbone-interrupted but geometrically continuous B-form DNA helices through base-pair stacking interactions that engage when the two opposing and cantilevered blunt-end arrays come into contact (Fig. 1C, bottom inset). The design also allows controlling the number and the sequences of the interfacial base pairs (fig. S2). In total, we prepared 50 distinct variants (figs. S3 to S8) that sampled all 16 possible combinations of installing a particular interfacial base-pair type on the array on the left beam and another type in the array on the right beam. Some of those variants were identical at the interface (dyad pairs with point-mirrored sequences), which we considered a desirable redundancy. For each particular sequence combination, we created arrays with two, four, and six blunt ends on either beam interface. Each blunt end in an array had the same terminal base-pair sequence. For the sequence combinations (TA:GC) and (GC:TA) we also created arrays with eight interfacial blunt-end contacts.

TEM imaging

To illustrate the function of the tethered-beam variants, we imaged exemplarily several variants (figs. S9 and S10) using negative-staining transmission electron microscopy (TEM). One control variant ("open"); (fig. S10C) lacked interfacial blunt ends (Fig. 2A). The TEM data of the open variant shows flexibly tethered particles where the orientation of one beam correlates poorly with the orientation of the other beam of the construct. Another control variant ("hybridized") (fig. S10B) had stable double-helical connections

¹Labor für Biomolekulare Nanotechnologie, Physik Department and Walter Schottky Institute, Technische Universität München, Am Coulombwall 4a, Garching near Munich, Germany. ²Lehrstuhl für Molekulare Biophysik, Physik Department, Technische Universität München, James-Franck-Strasse 1, Garching near Munich, Germany. ³Munich Center for Integrated Protein Science, 81377 Munich, Germany. ⁴Institute for Advanced Study, TUM, Germany.

*Corresponding author. Email: dietz@tum.de

between the two beams, as realized via four complementary sticky ends that bridge the two beams (Fig. 2B). TEM data of the hybridized variant revealed particles with a rigid-beam-like appearance in which the orientation of one beam correlates strongly with that of the other beam. Finally, we also imaged several of our stacking variants (Fig. 2C) [see also figs. S11 and S12 for images of other variants with the longer beams used in the single-molecule mechanical experiments (28)]. In the TEM data obtained with stacking variants, we observed both open particles and particles with a rigid-beam-like appearance resembling those of the hybridized variant. The appearance of the linkage between the beams agreed well with the expected appearance based on the design of the variant (see arrows in Fig. 2, B and C). The TEM data therefore supports that our tethered-beam particles featuring arrays of blunt ends function as desired: When the stacking bonds between the beam interfaces are engaged, a rigid-beam-like state is adopted in which the stacking mediates geometrical and mechanical properties that are similar to those mediated by continuous double-helical DNA domains. If the stacking bonds are broken, the particles extend and become much more flexible.

Electrophoretic mobility analysis

The difference in effective size of the particles with engaged versus open stacking bonds affects their electrophoretic mobility (fig. S13), which

allowed us to analyze the conformational equilibrium of the full 500-nm-long stacking variants on the ensemble level in a gel shift assay (Fig. 2D). Twenty-seven variants migrated in a sharp band with the high mobility that is associated with the closed, rigid-beam-like conformation [e.g., 4x (AT:CG) and 6x (AT:CG)]. Thirteen variants migrated in a band with the low mobility that corresponds to the open, flexible conformation [e.g., 2x (CG:AT) and 4x (CG:AT)]. Ten variants migrated in a less-well-defined band, with mobility in between those of the open and the closed conformation. The gel data reflects a strong dependency of the conformational equilibrium on the particular stack sequence combination, as previously seen for individual nicked DNA duplexes (29) and on the array size in a variant. When sorting the gel lanes according to the mobility of the leading band (Fig. 2E), going from low mobility (open states, weak stacking) to high mobility (closed states, strong stacking), it becomes apparent that the greater the number of stacking bonds in a variant, the more sequence combinations firmly populate the closed state, reflecting the desired avidity effects.

Mechanics of stack arrays and lifetime measurements

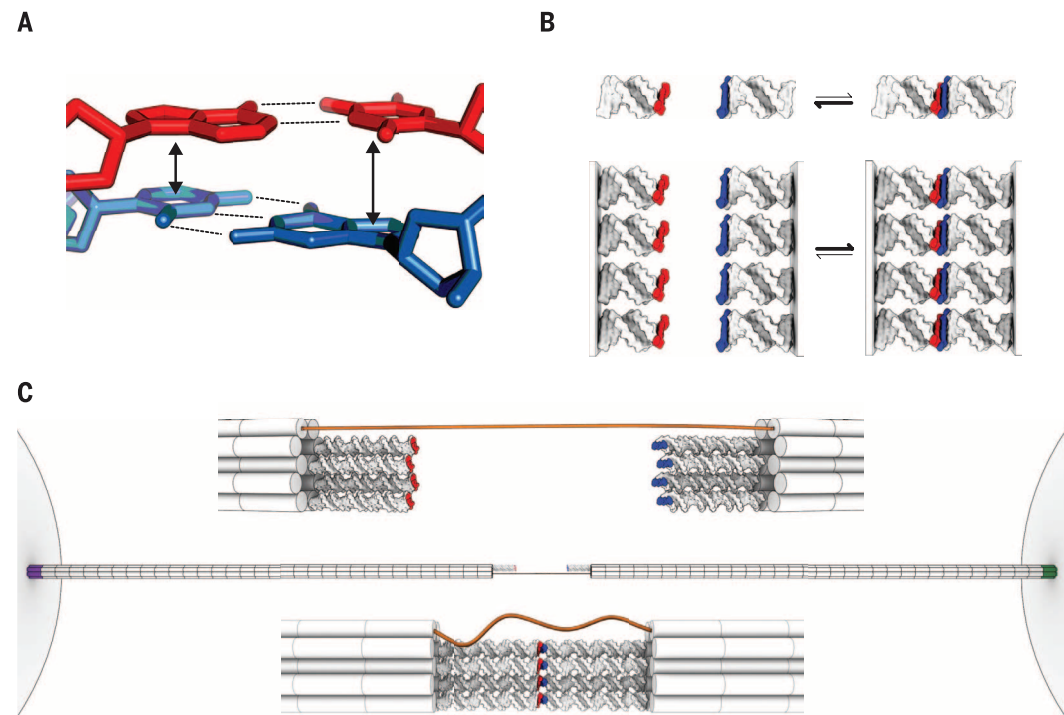
We used a dual-beam optical trap to study the force-extension response and the force-dependent transition kinetics of our stacking variants on the single-particle level. Consistent with their design, the stacking variants exhibited the nonlinear force-

extension response of multihelix bundles (20) and reversible transitions between a short and noise-reduced state and a longer, noise-enhanced state (Fig. 3A). The change in extension was consistent with the properties of the designed tether (figs. S14 and S15). The difference in noise amplitude at the same forces (Fig. 3A, red arrows) reflects the reversible change in the mechanics of the particles between the shorter, rigid-beam-like state with closed stacks and low noise and the extended, more flexible state with broken stacks and increased noise. Exemplary force-extension data obtained for the four base-pair stacking configurations that may be created with the two bases A and T, namely (AT:TA), (TA:AT), (AT:AT), and (TA:TA) illustrate the broad spectrum of mechanical stability and transition kinetics that we observed among the variants studied, including saw-tooth-like out-of-equilibrium unstacking at high forces and restacking at low forces (Fig. 3A) over close-to-equilibrium flips at intermediate forces (Fig. 3, B and C) to plateau-like rapid equilibrium transitions at low forces (Fig. 3D). The force versus extension data verified the integrity of our stacking variants but was not evaluated to extract bond lifetimes.

Instead, to focus on the particular force regime at which transitions occur as seen in the force versus extension data (Fig. 3, B and C, insets), we studied the stacking variants at different, but constant, trap distances. At each constant trap distance, we observed transitions between the open and closed states and measured the time

Fig. 1. Exploring base-stacking forces on the single-molecule level.

(A) Schematic depiction of two consecutive base pairs within a B-form double-helical domain. Helix axis is oriented vertically. Arrows, stacking interactions; dashed lines, hydrogen bonds. **(B)** (Top) Schematic illustration of the interaction of blunt-end double-helical DNA through stacking. Red, blue: terminal base pairs that form the stacking contact. The interaction is weak; it takes ~150 mM duplex concentration to effectively populate the bound state (55). (Bottom) Avidity effects in arrays of parallel blunt ends will shift the equilibrium. **(C)** Schematic illustration of the tethered-beam platform attached to two micrometer-sized beads via biotin-streptavidin (purple) and digoxigenin-antidigoxigenin (green) linkages (see fig. S3 for details) (28). Beads are drawn at $\sim 1/5$ of the actual radius. Beams are formed from 10 parallel DNA double



helices arranged in honeycomb packing (22). The tether (orange) is a [T]68 single strand. (Top inset) Zoom-in showing the system in the open state with stretched tether. The interfaces are functionalized; the configuration shown has four cantilevered blunt-end DNA double helices. Terminal base pairs are in helical register within an array. The change in helical twist between red and blue corresponds to those in B-Form DNA. (Bottom inset) Zoom-in showing the closed, bound state with geometrically continuous B-form double helices that are stabilized via stacking interactions between the blunt ends.

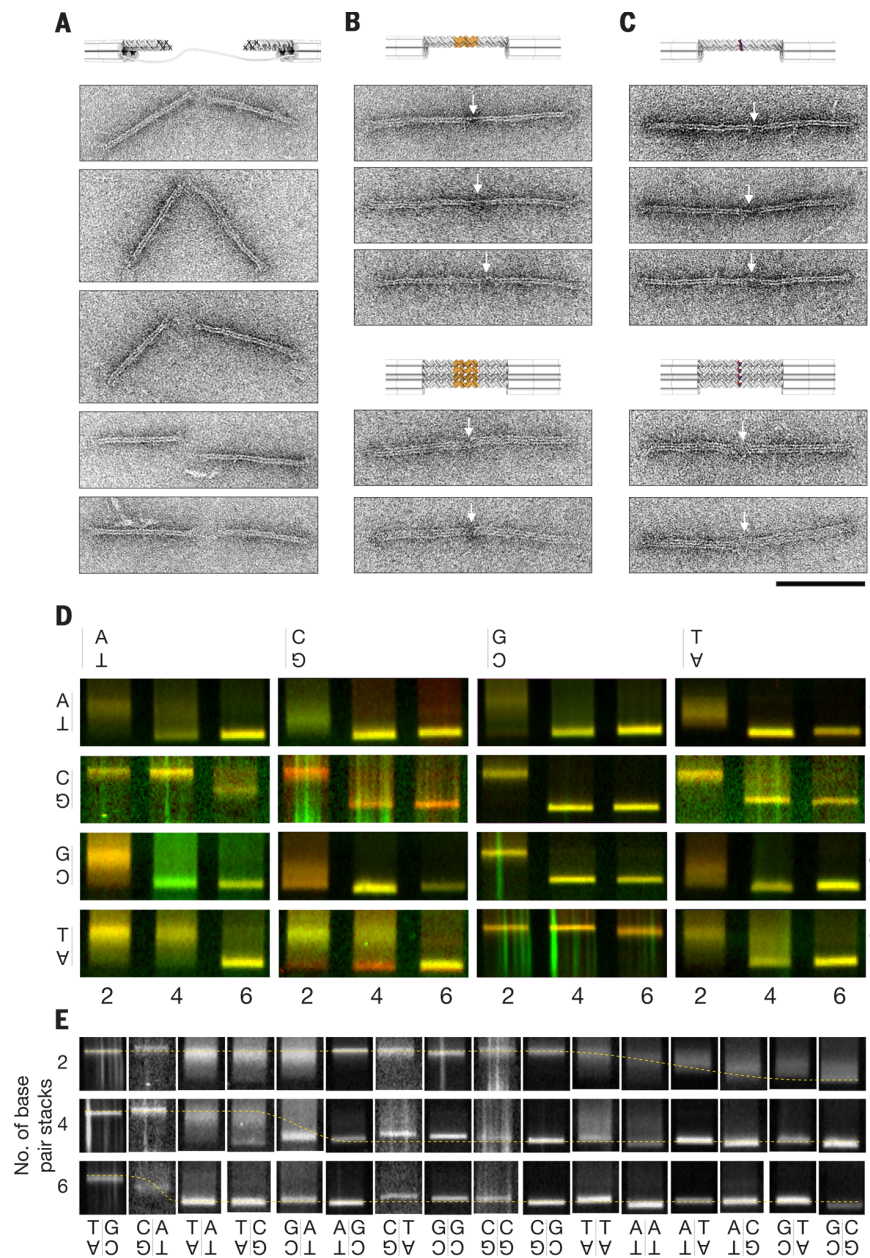


Fig. 2. TEM images and gel electrophoretic mobility. Typical negative-staining TEM micrographs. (A) A control variant with passivated interfaces. (B) A control variant with four cantilevered DNA domains on each beam stably connected by 3-base-pair-long sticky end interactions. (C) A dynamic stacking variant with four blunt-end stacking contacts (GC:CG) in the closed, bound state. Arrows indicate the interfacial helix sheet. Scale bar, 100 nm. The variants used in optical trapping experiments were twice as long and were produced by dimerization of two separate DNA origami beams (see materials and methods and figs. S4 to S10) (28). (D) Laser-scanned, channel-merged, false-colored images of agarose gels on which tethered-beam platform variants with stacking contacts were electrophoresed. One beam was labeled with Cy5 (red), the other with Cy3 (green). The data shown were collected from three different gels. Sequence combinations are given such that rows and columns give the identities of the left versus right base pair in our nomenclature. Numbers indicate array size. For example, the top left triple denotes samples with 2, 4, and 6 (AT:AT) stacks. “o” versus “c” indicates mobility of open versus closed states. (E) Individual gel lanes were cropped from the gel images and sorted according to the electrophoretic mobility of the leading band. Dashed line: guide to the eye that interpolates the position of the leading band, highlighting the shift in the equilibrium from open to closed states. Variants with (AT:GC), (CG:TA), (GC:GC), (CG:CG), and (CG:GC) had comparable mobilities within the same array size class and cannot be unambiguously sorted.

the system dwells in each of the two states (Fig. 3, E and F). The equilibrium between the two states, as well as the force exerted on the particles in each conformational state, depends on the particular value of the constant trap distance. This type of experiment is suited particularly for measuring rapid transitions without limitations from the finite delay time of a force-feedback system (30). It enabled us to determine stacking lifetimes over four orders of magnitude, ranging from milliseconds to several seconds (Fig. 3G), where the system became limited by drift and other disturbances. Altogether, 31 out of 50 variants gave measurable transitions in the presence of 20 mM magnesium chloride, where the remaining variants either were too stable or too fragile to collect transitions with our assay. Among those variants were all 16 possible stacking sequence combinations (when taking into account identity of left versus right beam). Fifteen sequence combinations occur in two different array sizes, either two and four, four and six, or six and eight stacks. For another subset of nine variants, we also collected lifetime versus force data in the presence of 500 mM sodium chloride, which is a model for the physiological concentration of monovalent cations in the cell nucleus (31). To extract the lifetimes of the stacked and unstacked states as a function of force, we analyzed in total more than two million dwells. The transition statistics varies among the dynamic stacking variants because of fast versus slow kinetics.

Force-dependent transition kinetics of stack arrays

The average lifetimes of the unbound states with extended tether and broken stacks were comparable (within experimental error) across all variants that we tested (figs. S16 to S18). This observation indicates sequence-independent rebinding rates. The rebinding of the stack arrays also had a pronounced dependency on force, which may be understood by considering that rebinding of the stacks requires a thermally activated contraction of the flexible tether—which was the same for all variants—against an opposing force.

The average lifetimes of the stacked states, however, provided a much more diverse picture (Fig. 4, A and B). The total range of lifetimes of the stacked states covers almost five orders of magnitude, from milliseconds to tens of seconds. Larger array sizes always have substantially longer lifetimes than smaller array sizes for a given base-pair step sequence combination, consistent with the expectation based on avidity. We note that in the case of larger array sizes, partial restacking with lateral shifts in the stacking contacts may occur occasionally. The lifetime data also reflect a strong dependency of unstacking on the particular sequence combination of the base-pair steps (Fig. 4A). Consider the stark contrast in the kinetics of unstacking (TA:GC) versus (GC:CG) base-pair steps: Six (TA:GC) steps in parallel together still make only quite transient bonds that last on average less than 10 ms. By contrast, two (GC:CG) steps were already much more stable and lasted nearly 1 s. In fact, (GC:CG) base-pair

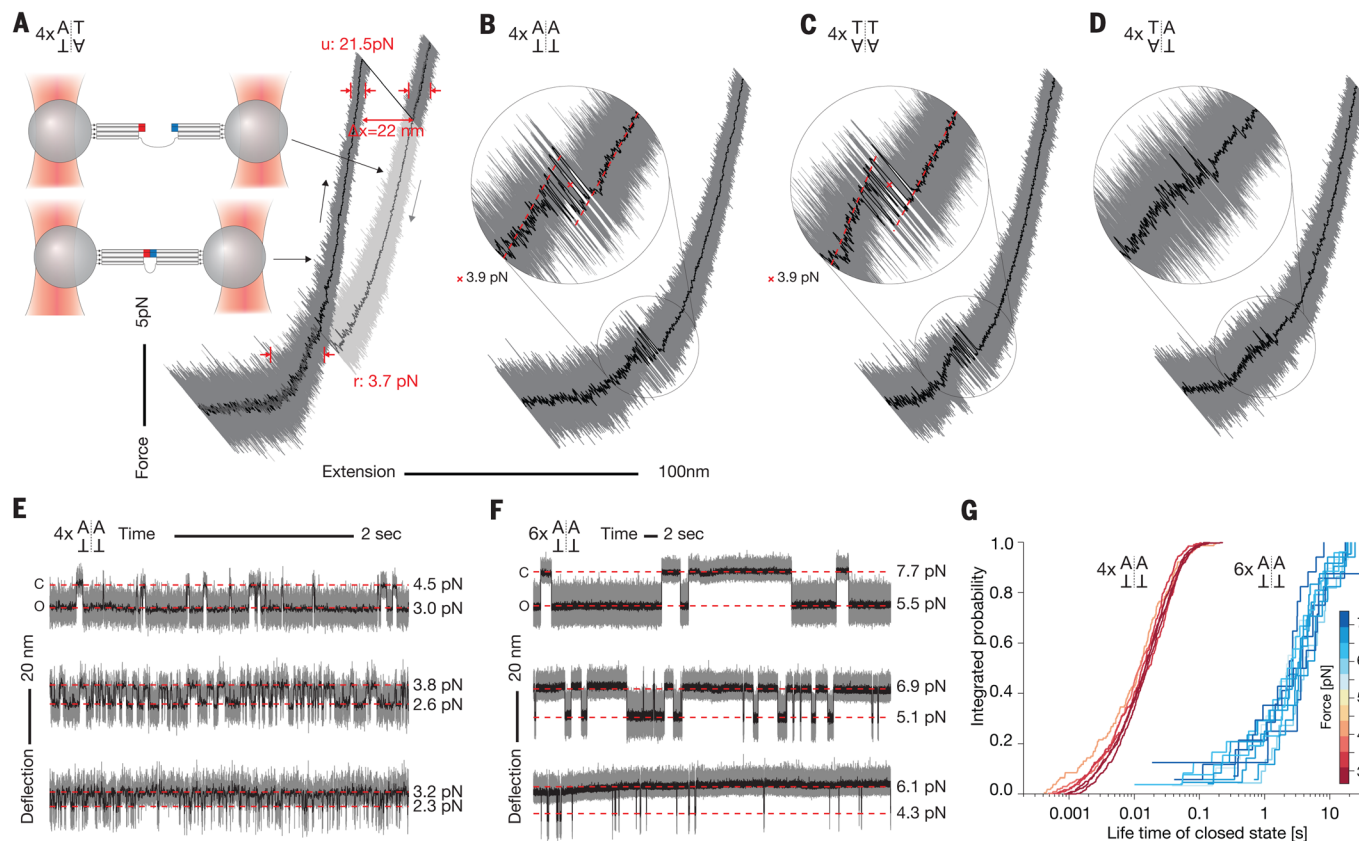


Fig. 3. Force-extension and constant-distance data of single tethered-beam particles featuring stacking contacts. (A) Exemplary force-extension data of a single tethered-beam particle with four (AT:TA) stacking contacts, as measured in a dumbbell assay with a dual-beam optical trap (inset). Dark gray, stretching; light gray, consecutive relaxing. Upon stretching, a rupture transition (marked with “u”) occurs at 21.5 pN, leading to an extension gain Δx that is consistent with wormlike chain lengthening of the [T]68 tether. Upon relaxing, a snap (marked with “r”) back to the shorter state with closed stacks occurs at 3.7 pN. The noise amplitudes are smaller in the shorter, closed state than in the longer, open state (see red arrows) due to greater stiffness of the closed state. (B to D) Exemplary force-extension data of single particles featuring the other three possible stacking combinations of A and T in arrays with four stacks. Insets show the transition

regime. The point-mirrored combinations (AT:AT) versus (TA:TA) [(B) versus (C)] have comparable mechanics featuring multiple close-to-equilibrium transitions (see insets) occurring at 4 pN. The least stable variant (TA:AT) unstacks and restacks in apparent equilibrium as reflected in a plateau-like transition. (TA:AT) is sequence-swapped compared with the (AT:TA) variant [see (A)]. (E and F) Constant trap-to-trap distance data of single particles with four versus six (AT:AT) stacking contacts. The particles transition reversibly between two states. “c” and “o” denote the shorter, closed state with intact stacking bonds versus the longer, open state, respectively. Increasing the force reduces the frequency of occurrence and the duration of the stacked states (bottom to top). The increase in array size from four to six stacks has a drastic effect on the overall transition kinetics. (G) Cumulative dwell time histogram of the closed states with intact stacking bonds.

steps had such long lifetimes that we had to change the salt concentration to study transitions with variants that had more than two (GC:CG) contacts (Fig. 4B). Together, the kinetic data now allows ranking base-pair steps according to their force-dependent lifetime. Because we did not detect appreciable differences in the rebinding rates, this kinetic ranking also reflects a ranking according to thermodynamic stability. From the lifetime data in Fig. 4, designers of DNA-based nanoscale devices (7, 32) can directly read off the expected lifetimes of stack arrays for all sequence combinations and for various array sizes and at salt conditions that are commonly used in the field. The data thus provides design solutions that cover orders of magnitude from milliseconds to several seconds.

Dyads and swapped base pairs

Among the sequence combinations that we tested were six pairs having point-mirrored sequence combinations (“dyads”) such as (AT:CG) versus

(GC:TA) (see fig. S19A for a scheme). The type and the relative orientation of molecular surfaces that interact in the point-mirrored pairs are identical. The dyad pairs had comparable force-dependent lifetimes within one order of magnitude in the single-particle measurements (Fig. 4 and fig. S19), and they also had comparable electrophoretic mobility patterns in ensemble (Fig. 2). The similar behavior of dyad pairs points against significant influences from phenomena such as fraying on the association and dissociation, because fraying is expected to depend on the type of neighboring base pairs located next to the terminal base pairs within the cantilevered stack arrays, but the neighbors were different within the dyad pair designs. There were also six swapped-sequence pairs such as (AT:CG) versus (CG:AT) (see fig. S19A for a scheme). Even though the base-pair composition was the same, buried versus exposed molecular surfaces were interchanged in swapped-sequence pairs. Our data revealed that swapping the sequence led to strong differences in the lifetime

of the stacking interaction, because five out of six swapped sequence pairs had lifetime differences that spanned several orders of magnitude (fig. S20). The data on swapped sequence pairs underlines the sensitivity of our assay for the details of the interfacial stacking interactions.

Low force sensitivity

Another feature revealed in our lifetime data is the overall low sensitivity of stacking contacts on the extent of pulling force in the helical direction. Increasing the force by 2 pN on the most force-sensitive of our stacking variants (TA:CG) leads to a lifetime reduction by merely a factor of 3. The most insensitive variant was the one with four (CG:CG) stacks whose lifetime was essentially independent of the applied force. Therefore, pulling on DNA base-pair stacks along the helical direction with biologically relevant forces in the <10-pN range hardly accelerated stack dissociation. The low force dependence indicates short-range interactions with transition states in subnanometer

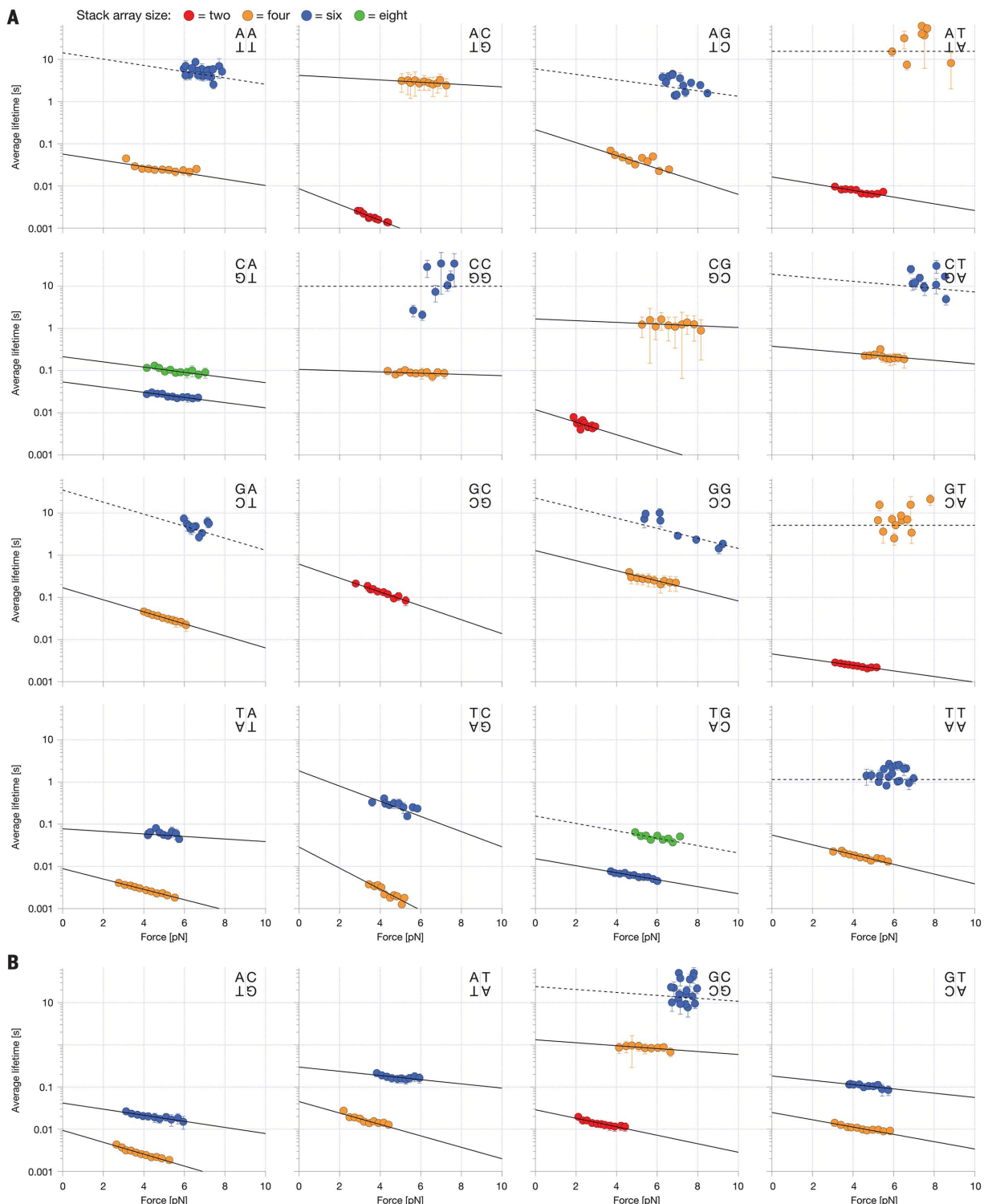


Fig. 4. Average lifetime of base-pair stack arrays as a function of force.

(A and B) Average stack array bound-state lifetime versus applied force data branches as determined from single particle data obtained in the presence of 20 mM MgCl₂ (A) versus 500 mM NaCl (B) for all possible stack sequence combinations and for various array sizes (red circles, two stacks; orange circles, four stacks; blue circles, six stacks; green circles, eight stacks). Solid lines are exponential fits. For the variants with particularly long lifetimes in the >1 s regime, drift and optical trap contamination limited the overall measurement time, which in turn resulted in low transition statistics per force value. In these cases, no force-resolved lifetime averages were calculated. Instead, given the generally

weak dependency on force, we used the overall mean. Dashed lines give a guide to the eye. Note the effect of salt concentration on the average lifetime: e.g., the variant with four AT:TA stacks has the overall longest lifetime in 20 mM MgCl₂ but ranks among the variants with the shortest lifetime in the presence of 500 mM NaCl. The rebinding lifetime versus force data are given in figs. S16 and S17. See supplementary materials section 1.6.1 for details, figs. S29 to S31, and tables S1 to S5 for a list of parameters from individual fits and global fits (28). At a stacking contact, our constructs feature the phosphates contributed by the scaffold strand. Blunt-end forming DNA oligonucleotides did not contain terminal phosphates.

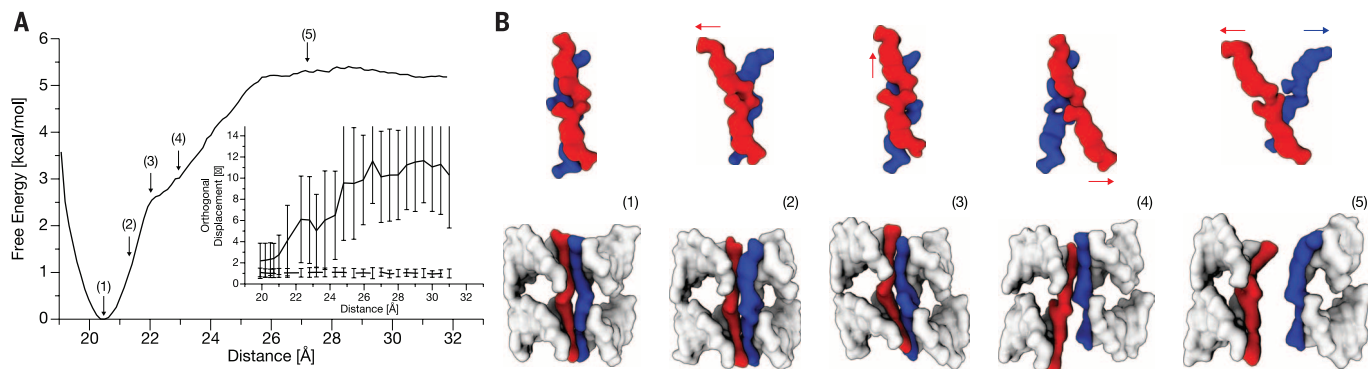


Fig. 5. Molecular mechanism of stack disruption. (A) The change in free energy was calculated for the disruption/formation of two (GC:CG) stacks along the axis perpendicular to the base-pair plane (helical axis) using umbrella sampling with molecular dynamics simulations (see supplementary materials section 1.5). The free energy approaches a minimum at a distance corresponding to the fully stacked configuration (~20.4 Å between centers of the two DNAs) and reaches a plateau upon complete dissociation (>26 Å). (Inset) Calculated average displacement in Angstroms (orthogonal to the helical axis) of the two terminal base

pairs on the other beam interface [illustrated in red and blue in (B)]. Disruption of stacking results in a steep rise of displacements orthogonal to the pulling direction (bold line) compared to mean base-pair displacement within an intact helix (shown for comparison as a dashed line; error bars indicate standard deviations of the mean). (B) Snapshots of the dynamics of the two interacting base pairs (indicated in red and blue, respectively) corresponding to the labeled positions in the free-energy plot shown in (A). The top row is the view along the helical axis, showing only the interfacial base pairs. Arrows indicate displacement directions (orthogonal to the direction of stacking disruption/formation).

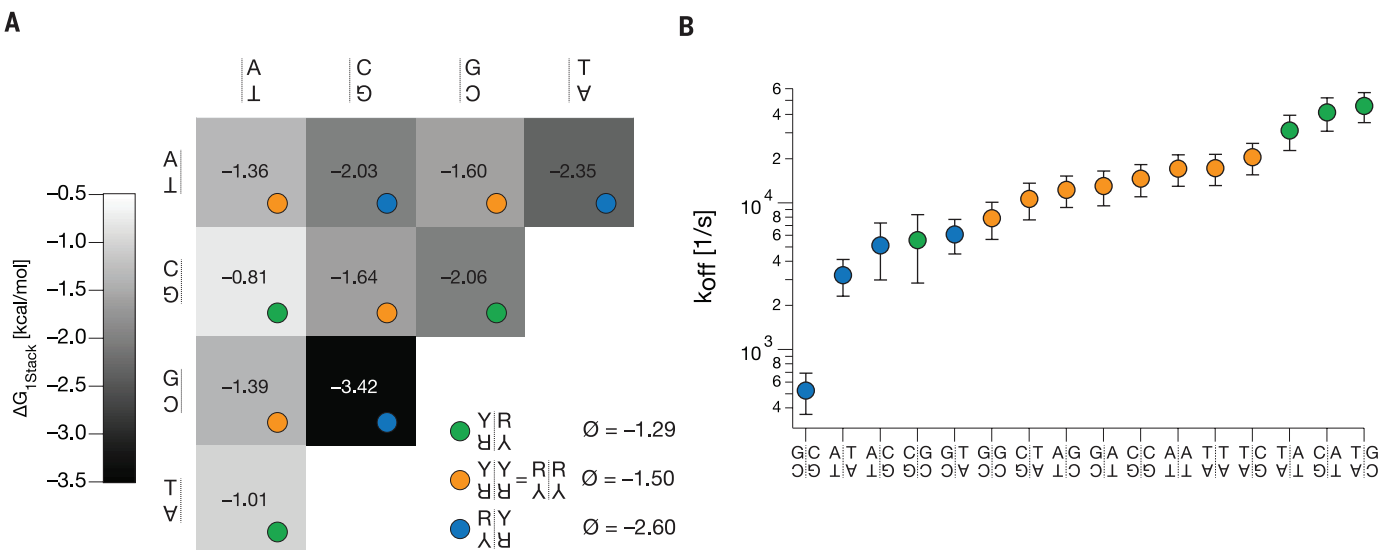


Fig. 6. Energetics and kinetics of base-pair stacking. (A) Single-stack free-energy increments for closing the 10 unique base-pair steps, as derived from single-molecule two-state association and dissociation rates in equilibrium (see supplementary materials section 1.6.2). The estimate uses $1.7 \times 10^5 \text{ s}^{-1}$ as the global association rate, which was obtained through trap-stiffness-corrected extrapolation of rebinding data to zero force (30, 50). Colored dots give stack classification according to underlying chemical backbone. We estimate the error per value to about $\pm 0.2 \text{ kcal/mol}$; see fig. S22. (B) Symbols: single-stack dissociation rates at zero force. See supplementary materials section 1.6.2 and table S6. Bars give propagated statistical error of the extrapolation to zero force in Fig. 4, A and B.

distances to the bound states (33). The low force sensitivity of stacking bonds observed herein may be contrasted with the much larger force sensitivity for unzipping of nucleic acid hairpins (19), where transition state distances depend on the sequences and stem lengths of the hairpins and can be several nanometers long, as expected for transitions that involve the breaking of several base pairs and base-pair stacks in series.

Molecular mechanics of stack disruption

To study the molecular details associated with the disruption of a blunt-end stack and to address the origin of the insensitivity of unstacking base-

pair steps through axial pulling forces, we investigated exemplarily (CG:GC) base-pair step disruption using molecular dynamics umbrella sampling (Fig. 5). Two (CG:GC) base-pair step stacking units were disrupted along a helical axis pulling direction, allowing calculation of a potential of mean force (PMF) (free energy change) along the direction of separation (Fig. 5A). The PMF was comparable to those computed previously for the end-to-end attraction between individual DNA duplexes (34). The free-energy change reached a plateau upon separation by ~0.6 nm relative to the free-energy minimum (unstacking completed). The magnitude of the calculated PMF depends on

the restraints to align the DNA molecules with respect to the pulling direction [see methods for details (28)]. A sequential disruption of the two blunt-end stacks was observed (disruption of the first base-pair stack at ~0.3 nm separation). Interestingly, during the onset of the dissociation of the first blunt-end stacking contact, a dramatic increase in the base-pair motion orthogonal to the pulling direction was already observed (Fig. 5A, inset), with amplitudes much larger than the shift-and-slide motion of a regular base-pair stacking contact. The orthogonal motions increased even further during disruption of the second blunt-end stack (see snapshots in Fig. 5B). We

conclude that the motions orthogonal to the pulling direction promote onset of dissociation caused by stack overlap reduction, similar to that seen previously for the end-to-end dissociation of individual DNA duplexes (34). Because the motions occur orthogonally to the direction of the applied force, they are hardly influenced by the actual magnitude of the force, which concurs with our experimental observation of force-insensitive unstacking kinetics (Fig. 4, A and B).

Discussion

Because we have measured forward and backward rates of arrays of base-pair stacks in equilibrium, we can attempt an estimate of the equilibrium free-energy differences for unstacking a single base-pair step. To this end, we use a constant rebinding rate informed by our experimental observation of comparable rebinding kinetics independent of sequence and array size (figs. S16 to S18), and we use average bound-state lifetimes extrapolated to zero force (Fig. 4). For our estimate, we further assume additive free energies per stacking bond within an array, and we ignore a potential penalty for forming the bound state. Based on the rates and these assumptions, we computed the free-energy increments per single stack for all stack arrays that we measured (supplementary materials section 1.6.2). The free energy increments per stack were largely independent of the total number of stacks, and there is no clear trend visible that argues against our simplifying assumptions (fig. S21). The free-energy differences obtained from different array sizes were averaged, and the energies from dyad sequences were also averaged. The free-energy increments that we thus obtained (Fig. 6A) from our single-molecule transition rates in equilibrium and under native solution conditions correlate well with those obtained previously from ensemble experiments with nicked DNA duplexes under denaturing conditions at low ionic strength (see figs. S22 and S23) (28, 35). We consider the agreement between the two parameter sets as remarkably good, given the strongly differing experimental approaches. However, aside from our simplifying assumptions, our estimates are also affected by force-calibration uncertainties (36). We use the deviations from an ideal linear relationship between our parameters and those obtained previously (35) as a measure of the joint error from both measurements (see caption of Fig. 6 and fig. S22).

The single-stack free-energy increments show a trend with respect to the chemical backbone of the nucleobases: 3' pyrimidine interfaces stacked on 5' purines [as in (CG:AT) steps] form the weakest bonds. Combinations having purines on purines and pyrimidines on pyrimidines [as in (AT:AT) base-pair steps] have intermediate stability, while 3' purine interfaces stacked on 5' pyrimidines [as in (GC:CG) or (AT:TA)] form the strongest bonds. This hierarchy is not visible in the next-neighbor base-pairing free-energy parameters derived previously from ensemble duplex melting (37), presumably because these parameters give the joint contribution from stacking and hydrogen-

bonding forces (figs. S22 and S23) (28). The trend in the stacking-strength hierarchy may be associated with the extent of geometrical atomic overlap between the bases within a base-pair step (see, for illustration, fig. S24) (28), which also holds for the outlier from the chemical backbone hierarchy trend [(CG:GC) in Fig. 6A].

The data obtained experimentally with multiple base-pair stacks in parallel enable estimating the average dissociation rates for a single stack (Fig. 6B). For the estimate, we considered the stack arrays as a two-state system with additive energies per stack, as above. The statistical treatment as a two-state system is supported by the observation that the lifetimes of many of the variants that we studied were distributed in a single exponential fashion. In particular, for arrays with six and eight stacks, deviations from a two-state-like behavior could have been expected due to large bond numbers, which was not the case. According to our estimate, the bonds between individual base-pair stacks break stochastically with average rates that vary between 500 s^{-1} for the most stable (GC:CG) combination and up to $50,000\text{ s}^{-1}$ for the most transient combinations (TA:AT), (CG:AT), and (TA:GC). The average dissociation rate per base-pair stack is on the order of 15 thousand events per second at our conditions. The dissociation and association rates are salt dependent (figs. S25 and S26). We note that the estimated single-stack dissociation rates are consistent with the high speeds at which DNA replication occurs *in vivo* (e.g., several thousand base pairs per second in *Escherichia coli*). Given also our finding that forces below 10 pN in the helical direction do not substantially accelerate the breaking of base-pair stacks, we speculate whether stepwise strand separation during the replication could be considered as a Brownian-ratchet-like process with forward bias, in which the enzymes involved exploit spontaneous DNA base-pair-stack opening, rather than actively breaking DNA base pairs in the helical direction. However, forces orthogonal to the helical direction could potentially have a strong influence on destacking kinetics.

Assuming that the sequence dependence of DNA double-strand formation is determined by differences in stacking and base pairing (mainly hydrogen bonding), one can use next-neighbor DNA stability parameters (37) and our stacking parameters to estimate the hydrogen bonding contribution. However, the analysis involves a salt correction (38), and the calculated hydrogen bonding contribution can only be interpreted as an extracted trend (fig. S27) (28). According to this trend, the hydrogen bonding contribution is more favorable for GC than for AT base pairs.

Outlook

Our experimental methods that use molecularly precise DNA origami components expand the capabilities of single-molecule mechanical experiments. Target molecular surfaces may be placed and exposed in controlled orientations and stoichiometry to study the weak forces occurring between them in solution. A variety of interactions

between various kinds of molecules may be studied in the future, due to the modularity and the addressability of the DNA origami-based tethered-beam system. The sequence-resolved kinetic information obtained in our experiments may inform models of DNA hybridization that are currently being developed (39). The insights obtained about stacking forces may help adjusting force fields to perform more realistic molecular dynamics simulations (40). Our data also provides a quantitative basis for the rational design of dynamic DNA-based nanoscale machines and assemblies (7, 32, 41), because the stacking free energies and the kinetic parameters can inform the design of conformational equilibria and the timing of transition kinetics according to user specifications.

Materials and methods

Design and preparation of tethered-beam platforms

The tethered-beam platforms were designed with caDNAno v0.1 (23). The two beams were folded individually, then agarose-gel purified, dimerized, and the dimers were again agarose-gel purified. Staple oligonucleotides (each at 200 nM) and the scaffold DNA (50 nM) were mixed in folding buffer containing 1 mM EDTA, 5 mM NaCl, 5 mM TRIS-Base, and 20 mM MgCl₂ at pH 8. Before the dimerization incubation, the concentration of the constructs was increased about five-fold using a PEG-precipitation step (42).

Electrophoretic ensemble analysis

The variants were electrophoresed on agarose gels after the dimerization reaction. The gels were laser-scanned in two channels (excitation at 635 nm, emission >665 nm, and excitation at 532 nm, emission between 520 nm and 540 nm) to measure the fluorescence of the dye labels included on each of the two beams of the tethered-beam platform.

TEM

5 μl of sample solution was applied to the carbon side of formvar-supported plasma-cleaned Cu400 copper grids (Science services) and incubated for 0.5 to 3 min. The samples were stained with a 2% uranyl formate solution containing 25 mM sodium hydroxide. The structures were imaged with a Philips CM100 electron microscope operated at 100 kV equipped with an AMT 4 Megapixel CCD camera.

Single-molecule measurements

Experiments were performed with a custom-built optical tweezers setup with back focal plane detection. The setup is described in detail elsewhere (24, 43). The calibration was performed as described previously (44). The measurements were conducted in a dumbbell assay (45, 46). The measurements were carried out in the presence of an oxygen scavenger system (47). State assignment was performed using either threshold analysis or using hidden Markov modeling (48). Force-dependent lifetimes of open and closed states of all measured variants were fitted with the Bell

Model (49). A previously described trap-stiffness correction was applied (30, 50).

Molecular dynamics free-energy simulations

For the generation of the starting structure, two B-DNA duplex molecules aligned along the z axis were placed in close vicinity with respect to the backbone segment of the central nucleotides (fig. S28). The generated new strand arrangement was energy minimized and solvated [TIP3P water (51)]. Neutralization of the system by addition of counter- and coions was done using the Amber14 package (52). The motion along the dissociation direction (z direction) was controlled by a quadratic center-of-mass distance restraint between the two segments. The free-energy change along the coordinate was calculated using the weighted histogram analysis method (53). The Curves+ program (54) was used for the analysis of helical fluctuations of the construct by treating the two stacked duplexes as two continuous helices in the Curves setup.

REFERENCES AND NOTES

- J. D. Watson, F. H. Crick, Molecular structure of nucleic acids: A structure for deoxyribose nucleic acid. *Nature* **171**, 737–738 (1953). doi: 10.1038/171737a0; pmid: 13054692
- E. T. Kool, Hydrogen bonding, base stacking, and steric effects in DNA replication. *Annu. Rev. Biophys. Biomol. Struct.* **30**, 1–22 (2001). doi: 10.1146/annurev.biophys.30.1.1; pmid: 11340050
- B. H. Robinson, C. Mailer, G. Drobny, Site-specific dynamics in DNA: Experiments. *Annu. Rev. Biophys. Biomol. Struct.* **26**, 629–658 (1997). doi: 10.1146/annurev.biophys.26.1.629; pmid: 9241432
- Y. Yin et al., Dynamics of spontaneous flipping of a mismatched base in DNA duplex. *Proc. Natl. Acad. Sci. U.S.A.* **111**, 8043–8048 (2014). doi: 10.1073/pnas.1400667111; pmid: 24843124
- S. F. Wickham et al., A DNA-based molecular motor that can navigate a network of tracks. *Nat. Nanotechnol.* **7**, 169–173 (2012). doi: 10.1038/nano.2011.253; pmid: 22266636
- B. Yurke, A. J. Turberfield, A. P. Mills Jr., F. C. Simmel, J. L. Neumann, A DNA-fuelled molecular machine made of DNA. *Nature* **406**, 605–608 (2000). doi: 10.1038/35020524; pmid: 10949296
- T. Gerling, K. F. Wagenbauer, A. M. Neuner, H. Dietz, Dynamic DNA devices and assemblies formed by shape-complementary, non-base pairing 3D components. *Science* **347**, 1446–1452 (2015). doi: 10.1126/science.aaa5372; pmid: 25814577
- J. J. Funke, H. Dietz, Placing molecules with Bohr radius resolution using DNA origami. *Nat. Nanotechnol.* **11**, 47–52 (2016). doi: 10.1038/nano.2015.240; pmid: 26479026
- H. Clausen-Schaumann, M. Rief, C. Toklsdorf, H. E. Gaub, Mechanical stability of single DNA molecules. *Biophys. J.* **78**, 1997–2007 (2000). doi: 10.1016/S0006-3495(00)76747-6; pmid: 10733978
- M. Rief, H. Clausen-Schaumann, H. E. Gaub, Sequence-dependent mechanics of single DNA molecules. *Nat. Struct. Biol.* **6**, 346–349 (1999). doi: 10.1038/7582; pmid: 10201403
- S. B. Smith, Y. Cui, C. Bustamante, Overstretching B-DNA: The elastic response of individual double-stranded and single-stranded DNA molecules. *Science* **271**, 795–799 (1996). doi: 10.1126/science.271.5250.795; pmid: 8628994
- Z. Bryant et al., Structural transitions and elasticity from torque measurements on DNA. *Nature* **424**, 338–341 (2003). doi: 10.1038/nature01810; pmid: 12867987
- J. Gore et al., DNA overwinds when stretched. *Nature* **442**, 836–839 (2006). doi: 10.1038/nature04974; pmid: 16862122
- J. M. Huguet et al., Single-molecule derivation of salt dependent base-pair free energies in DNA. *Proc. Natl. Acad. Sci. U.S.A.* **107**, 15431–15436 (2010). doi: 10.1073/pnas.1001454107; pmid: 20716688
- S. B. Smith, L. Finzi, C. Bustamante, Direct mechanical measurements of the elasticity of single DNA molecules by using magnetic beads. *Science* **258**, 1122–1126 (1992). doi: 10.1126/science.1439819; pmid: 1439819
- T. R. Strick, J. F. Allemand, D. Bensimon, A. Bensimon, V. Croquette, The elasticity of a single supercoiled DNA molecule. *Science* **271**, 1835–1837 (1996). doi: 10.1126/science.271.5257.1835; pmid: 8596951
- J. Lipfert et al., Double-stranded RNA under force and torque: Similarities to and striking differences from double-stranded DNA. *Proc. Natl. Acad. Sci. U.S.A.* **111**, 15408–15413 (2014). doi: 10.1073/pnas.1407197111; pmid: 25313077
- M. T. Woodside et al., Direct measurement of the full, sequence-dependent folding landscape of a nucleic acid. *Science* **314**, 1001–1004 (2006). doi: 10.1126/science.1133601; pmid: 17095702
- M. T. Woodside et al., Nanomechanical measurements of the sequence-dependent folding landscapes of single nucleic acid hairpins. *Proc. Natl. Acad. Sci. U.S.A.* **103**, 6190–6195 (2006). doi: 10.1073/pnas.0511048103; pmid: 16606839
- E. Pfitzner et al., Rigid DNA beams for high-resolution single-molecule mechanics. *Angew. Chem.* **52**, 7766–7771 (2013). doi: 10.1002/anie.201302727; pmid: 23794413
- P. W. Rothemund, Folding DNA to create nanoscale shapes and patterns. *Nature* **440**, 297–302 (2006). doi: 10.1038/nature04586; pmid: 16541064
- S. M. Douglas et al., Self-assembly of DNA into nanoscale three-dimensional shapes. *Nature* **459**, 414–418 (2009). doi: 10.1038/nature08016; pmid: 19458720
- S. M. Douglas et al., Rapid prototyping of 3D DNA-origami shapes with caDNAno. *Nucleic Acids Res.* **37**, 5001–5006 (2009). doi: 10.1093/nar/gkp436; pmid: 19531737
- Y. von Hansen, A. Mehlrich, B. Pelz, M. Rief, R. R. Netz, Auto- and cross-power spectral analysis of dual trap optical tweezer experiments using Bayesian inference. *Rev. Sci. Instrum.* **83**, 095116 (2012). doi: 10.1063/1.4753917; pmid: 23204248
- J. P. Junker, F. Ziegler, M. Rief, Ligand-dependent equilibrium fluctuations of single calmodulin molecules. *Science* **323**, 633–637 (2009). doi: 10.1126/science.11679531
- J. Kim, C. Z. Zhang, X. Zhang, T. A. Springer, A mechanically stabilized receptor-ligand flex-bond important in the vasculature. *Nature* **466**, 992–995 (2010). doi: 10.1038/nature09295; pmid: 20725043
- K. Halvorsen, D. Schaak, W. P. Wong, Nanoengineering a single-molecule mechanical switch using DNA self-assembly. *Nanotechnology* **22**, 494005 (2011). doi: 10.1088/0957-4484/22/49/494005; pmid: 22101354
- Materials and methods are available as supplementary materials on *Science Online*.
- E. Protozanova, P. Yakovchuk, M. D. Frank-Kamenetskii, Stacked-unstacked equilibrium at the nick site of DNA. *J. Mol. Biol.* **342**, 775–785 (2004). doi: 10.1016/j.jmb.2004.07.075; pmid: 15342236
- P. J. Elms, J. D. Chodera, C. J. Bustamante, S. Marqusee, Limitations of constant-force-feedback experiments. *Biophys. J.* **103**, 1490–1499 (2012). doi: 10.1016/j.bpj.2012.06.051; pmid: 23062341
- R. D. Moore, G. A. Morrill, A possible mechanism for concentrating sodium and potassium in the cell nucleus. *Biophys. J.* **16**, 527–533 (1976). doi: 10.1016/S0006-3495(76)85707-4; pmid: 1276381
- P. Ketterer, E. M. Willner, H. Dietz, Nanoscale rotary apparatus formed from tight-fitting 3D DNA components. *Science Advances* **2**, e1501209 (2016). doi: 10.1126/sciadv.1501209; pmid: 26989778
- E. Evans, K. Ritchie, Dynamic strength of molecular adhesion bonds. *Biophys. J.* **72**, 1541–1555 (1997). doi: 10.1016/S0006-3495(97)8802-7; pmid: 9083660
- C. Maffeo, B. Luan, A. Aksimentiev, End-to-end attraction of duplex DNA. *Nucleic Acids Res.* **40**, 3812–3821 (2012). doi: 10.1093/nar/gkr1220; pmid: 22241779
- A. Krueger, E. Protozanova, M. D. Frank-Kamenetskii, Sequence-dependent base pair opening in DNA double helix. *Biophys. J.* **90**, 3091–3099 (2006). doi: 10.1529/biophysj.105.078774; pmid: 16500982
- J. Stigler, F. Ziegler, A. Gieseke, J. C. Gebhardt, M. Rief, The complex folding network of single calmodulin molecules. *Science* **334**, 512–516 (2011). doi: 10.1126/science.1207598; pmid: 22034433
- J. SantaLucia Jr., D. Hicks, The thermodynamics of DNA structural motifs. *Annu. Rev. Biophys. Biomol. Struct.* **33**, 415–440 (2004). doi: 10.1146/annurev.biophys.32.110601.141800; pmid: 15139820
- R. Owczarzy, B. G. Moreira, Y. You, M. A. Behlke, J. A. Walder, Predicting stability of DNA duplexes in solutions containing magnesium and monovalent cations. *Biochemistry* **47**, 5336–5353 (2008). doi: 10.1021/bi702363u; pmid: 18422348
- N. Srinivas et al., On the biophysics and kinetics of toehold-mediated DNA strand displacement. *Nucleic Acids Res.* **41**, 10641–10658 (2013). doi: 10.1093/nar/gkt801; pmid: 24019238
- C. Maffeo et al., Close encounters with DNA. *J. Phys. Condens. Matter* **26**, 413101 (2014). doi: 10.1088/0953-8984/26/41/413101; pmid: 25238560
- S. Woo, P. W. Rothemund, Programmable molecular recognition based on the geometry of DNA nanostructures. *Nat. Chem.* **3**, 620–627 (2011). doi: 10.1038/nchem.1070; pmid: 21778982
- E. Stahl, T. G. Martin, F. Praetorius, H. Dietz, Facile and scalable preparation of pure and dense DNA origami solutions. *Angew. Chem.* **53**, 12735–12740 (2014). doi: 10.1002/anie.201405991; pmid: 25346175
- G. Žoldák, J. Stigler, B. Pelz, H. Li, M. Rief, Ultrafast folding kinetics and cooperativity of villin headpiece in single-molecule force spectroscopy. *Proc. Natl. Acad. Sci. U.S.A.* **110**, 18156–18161 (2013). doi: 10.1073/pnas.1314951110; pmid: 24145407
- S. F. Tolici-Nørrelykke et al., Calibration of optical tweezers with positional detection in the back focal plane. *Rev. Sci. Instrum.* **77**, 103101 (2006). doi: 10.1063/1.2356852
- J. W. Shaevitz, E. A. Abbondanzieri, R. Landick, S. M. Block, Backtracking by single RNA polymerase molecules observed at near-base-pair resolution. *Nature* **426**, 684–687 (2003). doi: 10.1038/nature02191; pmid: 14634670
- S. C. Blanchard, H. D. Kim, R. L. Gonzalez Jr., J. D. Puglisi, S. Chu, tRNA dynamics on the ribosome during translation. *Proc. Natl. Acad. Sci. U.S.A.* **101**, 12893–12898 (2004). doi: 10.1073/pnas.0403884101; pmid: 15317937
- M. P. Landry, P. M. McCall, Z. Qi, Y. R. Chemla, Characterization of photoactivated singlet oxygen damage in single-molecule optical trap experiments. *Biophys. J.* **97**, 2128–2136 (2009). doi: 10.1016/j.bpj.2009.07.048; pmid: 19843445
- J. Stigler, M. Rief, Hidden Markov analysis of trajectories in single-molecule experiments and the effects of missed events. *ChemPhysChem* **13**, 1079–1086 (2012). doi: 10.1002/cphc.201100814; pmid: 22392881
- G. I. Bell, Models for the specific adhesion of cells to cells. *Science* **200**, 618–627 (1978). doi: 10.1126/science.347575; pmid: 347575
- W. J. Greenleaf, M. T. Woodside, E. A. Abbondanzieri, S. M. Block, Passive all-optical force clamp for high-resolution laser trapping. *Phys. Rev. Lett.* **95**, 208102 (2005). doi: 10.1103/PhysRevLett.95.208102; pmid: 16384102
- W. L. Jorgensen, J. Chandrasekhar, J. D. Madura, R. W. Impey, M. L. Klein, Comparison of simple potential functions for simulating liquid water. *J. Chem. Phys.* **79**, 926–935 (1983). doi: 10.1063/1.445869
- D. A. Case et al., Amber14, University of California, San Francisco, CA (2014).
- S. Kumar, J. M. Rosenberg, D. Bouzida, R. H. Swendsen, P. A. Kollman, The weighted histogram analysis method for free-energy calculations on biomolecules. I. The method. *J. Comput. Chem.* **13**, 1011–1021 (1992). doi: 10.1002/jcc.540130812
- R. Lavery, M. Moakher, J. H. Maddocks, D. Petkovicite, K. Zukrowska, Conformational analysis of nucleic acids: revisited: Curves+. *Nucleic Acids Res.* **37**, 5917–5929 (2009). doi: 10.1093/nar/gkp008; pmid: 19625494
- M. Nakata et al., End-to-end stacking and liquid crystal condensation of 6 to 20 base pair DNA duplexes. *Science* **318**, 1276–1279 (2007). doi: 10.1126/science.1143826; pmid: 18033877

ACKNOWLEDGMENTS

We thank J. Stigler for technical assistance with data processing tools, P. Ketterer for help with illustrations, and J. P. Sobczak and J. Funke for discussions. F. Praetorius is acknowledged for scaffold DNA preparations. This work was supported by a European Research Council Starting Grant to H.D. (GA no. 256270) and by the Deutsche Forschungsgemeinschaft through grants provided within the Sonderforschungsbereich SFB863 [H.D. (project A9), M.R. (project A2), and M.Z. (project A10)] and the Gottfried-Wilhelm-Leibniz Program (to H.D.). Additional support came from the Nano Initiative Munich. F.K. was in part supported by a stipend from the Complin

program of Elitenetzwerk Bayern. Raw data that are not already included in the supplementary materials will be made available upon request. Author contributions: F.K. performed research; H.D. designed research. F.K., C.W., and H.D. analyzed and discussed data. B.P. and M.R. provided analytical tools and materials. M.Z. performed and analyzed molecular dynamics

simulations. F.K. and H.D. prepared figures and wrote the manuscript. F.K. and C.W. prepared the supplementary materials.

SUPPLEMENTARY MATERIALS

www.sciencemag.org/content/353/6304/aaf5508/suppl/DC1
Materials and Methods

Figs. S1 to S31
Tables S1 to S6
References

26 February 2016; accepted 1 July 2016
10.1126/science.aaf5508

EXTENDED PDF FORMAT
SPONSORED BY



Editor's Summary

Single-molecule dissection of stacking forces in DNA
Fabian Kilchherr, Christian Wachauf, Benjamin Pelz, Matthias Rief,
Martin Zacharias and Hendrik Dietz (September 8, 2016)
Science **353** (6304), . [doi: 10.1126/science.aaf5508]

This copy is for your personal, non-commercial use only.

Article Tools

Visit the online version of this article to access the personalization and article tools:
<http://science.scienmag.org/content/353/6304/aaf5508>

Permissions

Obtain information about reproducing this article:
<http://www.scienmag.org/about/permissions.dtl>

Science (print ISSN 0036-8075; online ISSN 1095-9203) is published weekly, except the last week in December, by the American Association for the Advancement of Science, 1200 New York Avenue NW, Washington, DC 20005. Copyright 2016 by the American Association for the Advancement of Science; all rights reserved. The title *Science* is a registered trademark of AAAS.